

## Quantum Interference of Electromagnetic Fields from Remote Quantum Memories

T. Chanelière, D. N. Matsukevich, S. D. Jenkins, S.-Y. Lan, R. Zhao, T. A. B. Kennedy, and A. Kuzmich

*School of Physics, Georgia Institute of Technology, Atlanta, Georgia 30332-0430, USA*

(Received 27 September 2006; published 16 March 2007)

We observe quantum, Hong-Ou-Mandel, interference of fields produced by two remote atomic memories. High-visibility interference is obtained by utilizing the finite atomic memory time in four-photon delayed coincidence measurements. Interference of fields from remote atomic memories is a crucial element in protocols for scalable entanglement distribution.

DOI: [10.1103/PhysRevLett.98.113602](https://doi.org/10.1103/PhysRevLett.98.113602)

PACS numbers: 42.50.Dv, 03.65.Ud, 03.67.Mn

Proposed approaches to scalable quantum-information networks and distributed quantum computing involve linear optical elements and single-photon detectors to distribute entanglement between remote parties [1–3]. For long-distance quantum networks transmission losses necessitate intermediate storage elements, quantum memories, which have the capability to faithfully store and retrieve quantum information, as has been demonstrated with cold atomic ensembles [4–6].

To connect independently entangled segments of a quantum network, and thereby distribute entanglement across it, it is necessary to perform joint measurements on neighboring elements of the network. Such entanglement connection may be achieved by the interference of photons, retrieved from these sites. The anticorrelation of photoelectric coincidence counts is the signature of Hong-Ou-Mandel interference (HOM), whereby indistinguishable single-photon wave packets simultaneously incident at two input ports of a beam splitter both exit in one or other of the output ports [7,8]. Observation of HOM for remotely generated, but indistinguishable, photons effects a Bell state measurement, leading to entanglement connection [9]. Several remarkable demonstrations of HOM using parametric down conversion have been reported (see Refs. [8,10,11], and references therein). It has also been observed using photon pairs generated locally by a single source—a quantum dot [12], an atom [13], and an atomic ensemble [14]. Recently HOM has been demonstrated with two (a) neutral atoms [15] and (b) ions [16], in each case separated by a few microns.

In this Letter we report HOM from two cold atomic ensembles located in adjacent laboratories and separated by 5.5 m (Fig. 1). We first outline how an atomic ensemble acts as a source of polarized photons correlated with orthogonal spin excitations of the ensemble [5]. Signal photons are generated by Raman scattering of a write laser pulse with temporal profile  $\varphi(t)$  [normalized to unity  $\int dt |\varphi(t)|^2 = 1$ ], whose length is much greater than the ensemble dimensions; see the inset to Fig. 1. Specifically, the atoms are prepared in the state  $|a, m\rangle$  with probability  $p_m = 1/(2F_a + 1)$ , corresponding to an unpolarized ensemble. Here  $|a\rangle$  and  $|b\rangle$  are the ground hyperfine levels

and  $|c\rangle$  is the excited level associated with the  $D_1$  line involved in the Raman process, with total angular momenta  $F_a$ ,  $F_b$ , and  $F_c$ , respectively, and we define  $X_{m,\alpha} \equiv C_{m0m}^{F_a 1 F_c} C_{m-\alpha m}^{F_b 1 F_c}$ , a product of Clebsch-Gordan coefficients, as a weight factor determining the relative strength of the Raman process between Zeeman sublevels  $|a, m\rangle$  and  $|b, m - \alpha\rangle$ .

To observe HOM, it is necessary that the photon wave packets be indistinguishable. Starting from a multimode description of the Raman process, we relate the detected signal fields to the driving write laser pulses, and fully account for the polarization properties of the interaction. We consider an unpolarized ensemble of  $N$  atoms interacting with an off-resonant vertically ( $\mathbf{e}_V = -\hat{z}$ ) polarized write field propagating in the  $y$  direction. The interaction picture Hamiltonian for the system includes a contribution representing Raman scattering into the detected signal mode defined by an optical fiber, and given by [17]

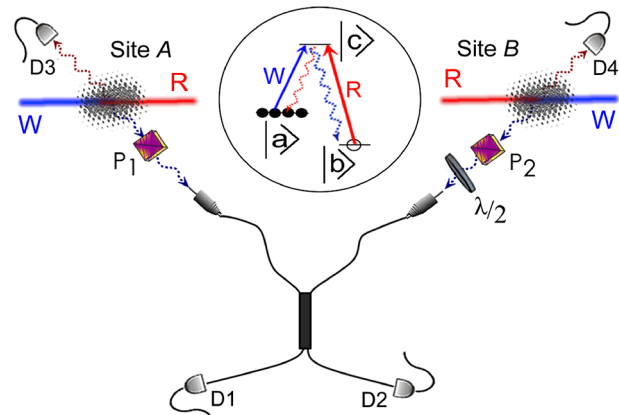


FIG. 1 (color online). Schematic showing Raman scattering of write pulses ( $W$ ) at sites  $A$  and  $B$  with signal fields collected by polarizers  $P_1$  and  $P_2$  and fiber beam splitter and directed towards detectors  $D1$ ,  $D2$ . A half-wave plate ( $\lambda/2$ ) may be inserted at site  $B$  to rotate light polarization. Raman scattering of delayed read pulses produces idler fields detected at  $D3$ ,  $D4$ . The inset shows the atomic level structure and the write- and read-induced Raman processes.

$$\hat{H}(t) = i\hbar\chi\varphi(t)[\cos\eta\hat{\psi}_H^\dagger(t)\hat{s}_H^\dagger + \sin\eta\hat{\psi}_V^\dagger(t)\hat{s}_V^\dagger] + \text{H.c.} \quad (1)$$

The parametric mixing angle  $\eta$  is given by [5,17]

$$\cos^2\eta = \frac{\frac{1}{2}\sum_{\alpha=\pm 1}\sum_m P_m X_{m,\alpha}^2}{\sum_m P_m X_{m,0}^2 + \frac{1}{2}\sum_{\alpha=\pm 1}\sum_m P_m X_{m,\alpha}^2}. \quad (2)$$

The annihilation operator for the Raman-scattered field emitted from the ensemble is given by  $\hat{\psi}_\lambda(t)$ ,  $\lambda = H, V$ . These field operators obey the usual free-field, narrow-bandwidth bosonic commutation relations  $[\hat{\psi}_\lambda(t), \hat{\psi}_{\lambda'}^\dagger(t')] = \delta_{\lambda,\lambda'}\delta(t-t')$ . The emission of  $H$ - or  $V$ -polarized signal photons creates correlated atomic spin wave excitations with annihilation operators  $\hat{s}_{H,V}$  given by  $\hat{s}_V = -\hat{s}_0$  and  $\hat{s}_H = \cos\theta\hat{s}_{-1} - \sin\theta\hat{s}_{+1}$ , where  $\cos^2\theta = \sum_m P_m X_{m,-1}^2 / \sum_{\alpha=\pm 1}\sum_m P_m X_{m,\alpha}^2$  and the spherical vector components of the spin wave are given by

$$\hat{s}_\alpha \equiv \sum_{m=-F_a}^{F_a} \frac{\sqrt{P_m} X_{m,\alpha}}{\sqrt{\sum_m P_m |X_{m,\alpha}|^2}} \hat{s}_{m,\alpha} (\alpha = \pm 1, 0).$$

The spin wave is defined in terms of the  $\mu$ th atom transition operators  $\tilde{\sigma}_{a,m;b,m'}^\mu(t)$  and the write  $\phi_w(\mathbf{r})$  and signal  $\phi_s(\mathbf{r})$  mode spatial profiles (normalized to unity in their respective transverse planes)

$$\hat{s}_{m,\alpha} \equiv \frac{i\mathcal{A}}{\sqrt{P_m N}} \times \sum_{\mu=1}^N \tilde{\sigma}_{a,m;b,m-\alpha}^\mu(t) e^{i(\mathbf{k}_s - \mathbf{k}_w) \cdot \mathbf{r}_\mu} \phi_s(\mathbf{r}_\mu) \phi_w^*(\mathbf{r}_\mu), \quad (3)$$

where  $\mathbf{k}_s$  and  $\mathbf{k}_w$  are the detected signal and write beam wave vectors, respectively, and  $\mathcal{A}$  is the effective overlap area of the write beam and the detected signal mode [17,18]. For a sufficiently large number of atoms  $N$  the spin wave operators  $\hat{s}_{H,V}$  can be treated as bosonic.

The dimensionless parametric coupling constant  $\chi$  is given by

$$\chi \equiv \frac{2d_{cb}d_{ca}}{\Delta} \frac{\sqrt{k_s k_w n_w N}}{\hbar\epsilon_0 \mathcal{A}} \sqrt{\sum_m P_m \left( X_{m,0}^2 + \sum_{\alpha=\pm 1} X_{m,\alpha}^2 / 2 \right)}, \quad (4)$$

where  $\Delta = ck_w - (\omega_c - \omega_a)$  is the write laser detuning from the  $c \leftrightarrow a$  transition,  $d_{cb}$  and  $d_{ca}$  are reduced dipole matrix elements for the  $c \leftrightarrow b$  and  $c \leftrightarrow a$  transitions,  $n_w$  is the average number of photons in the write pulse.

The interaction Hamiltonian also includes terms representing Rayleigh scattering, as well as the Raman scattering into undetected modes. One can show, however, that these commute with the signal Hamiltonian to order  $O(1/\sqrt{N})$  and that they commute with  $\hat{\psi}_\lambda$  and  $\hat{s}_\alpha$ . As a result, it is possible to trace over the unobserved field modes to arrive at the density operator for the correlated

signal field/spin wave system:  $\hat{\rho} = \hat{U}\hat{\rho}_0\hat{U}^\dagger$ . Here  $\hat{\rho}_0$  is the initial state of the unpolarized ensemble and vacuum electromagnetic field and the unitary operator  $\hat{U}$  is given by

$$\hat{U} = \exp(\chi \cos\eta \hat{a}_H^\dagger \hat{s}_H^\dagger + \chi \sin\eta \hat{a}_V^\dagger \hat{s}_V^\dagger - \text{H.c.}), \quad (5)$$

with the discrete signal mode bosonic operator  $\hat{a}_\lambda \equiv \int dt \varphi^*(t) \hat{\psi}_\lambda(t)$ , with commutation relation  $[\hat{a}_\lambda, \hat{a}_{\lambda'}^\dagger] = \delta_{\lambda,\lambda'}$ , where  $\lambda, \lambda' = H$  or  $V$ . We have thus reduced the multimode interaction of the electromagnetic field with an atomic ensemble to a parametric interaction of two discrete modes.

Using Eq. (5), the detected signal field operators  $\hat{a}_\lambda^{(\text{out})}$  can be computed in terms of the input signal and spin wave fields

$$\begin{aligned} \hat{a}_H^{(\text{out})} &= \hat{U}^\dagger \hat{a}_H^{(\text{in})} \hat{U} \\ &= \cosh(\chi \cos\eta) \hat{a}_H^{(\text{in})} + \sinh(\chi \cos\eta) \hat{s}_H^{(\text{in})\dagger}, \\ \hat{a}_V^{(\text{out})} &= \hat{U}^\dagger \hat{a}_V^{(\text{in})} \hat{U} \\ &= \cosh(\chi \sin\eta) \hat{a}_V^{(\text{in})} + \sinh(\chi \sin\eta) \hat{s}_V^{(\text{in})\dagger}. \end{aligned}$$

These solutions allow calculation of the photoelectric detection signals.

In this work, two magneto-optical traps (MOTs) of  $^{85}\text{Rb}$ ,  $A$  and  $B$ , located in adjacent laboratories, serve as the basis for remote quantum memory elements (Fig. 1). The signal field detected from ensemble  $A$ , generated by the write pulse with temporal profile  $\varphi_A(t)$ , is given by

$$\hat{E}_{\lambda,A}^{(+)} = \sqrt{\frac{\hbar k_s}{2\epsilon_0}} e^{-ick_s(t-(z_A/c))} \phi_{s,A}(\mathbf{r}) \varphi_A\left(t - \frac{z_A}{c}\right) \hat{a}_{\lambda,A}^{(\text{out})},$$

where  $z_A$  is a position coordinate. A similar expression is also valid for ensemble  $B$ .

The fields from  $A$  and  $B$  are combined on a beam splitter of reflectance  $R$  and transmittance  $T$ , with  $R + T = 1$ . Fields  $\hat{E}_{\lambda,1}$ ,  $\hat{E}_{\lambda,2}$  in the beam splitter output ports 1 and 2 are incident on detectors D1 and D2, respectively (Fig. 1). We employ vertically ( $V$ ) polarized write beams, derived from a single laser, and detect the horizontally ( $H$ ) polarized signal fields, which are passed through polarizing cubes prior to the beam splitter.

The corresponding cross-correlation function  $G_{\parallel}^{(12)}(t, t + \tau) \equiv \langle \hat{E}_{H,1}^-(t) \hat{E}_{H,2}^-(t + \tau) \hat{E}_{H,2}^+(t + \tau) \hat{E}_{H,1}^+(t) \rangle$  exhibits the HOM effect:

$$\begin{aligned} G_{\parallel}^{(12)}(t, t + \tau) &= \mathcal{E}_A^2 \mathcal{E}_B^2 |T \varphi_A(t + \tau) \varphi_B(t) \\ &\quad - R \varphi_B(t + \tau) \varphi_A(t)|^2 s_A^2 s_B^2 \\ &\quad + 2RT [\mathcal{E}_A^4 |\varphi_A(t + \tau) \varphi_A(t)|^2 s_A^4 \\ &\quad + \mathcal{E}_B^4 |\varphi_B(t + \tau) \varphi_B(t)|^2 s_B^4] \end{aligned} \quad (6)$$

where  $s_{A[B]} \equiv \sinh(\chi_{A[B]} \cos\eta)$ , and  $\mathcal{E}_{A[B]} = \sqrt{\hbar ck_s / (2\epsilon_0)} |\phi_{s,A[B]}(\mathbf{r})|$ . The first, HOM, term on the

right-hand side of Eq. (6) exhibits two photon interference and can be understood in terms of conventional single-photon interference conditioned on the first photoelectric detection at time  $t$  [13]. For zero delay  $\tau = 0$  and a symmetric beam splitter  $R = T = \frac{1}{2}$ , this term gives zero contribution even for  $\varphi_A \neq \varphi_B$ . Alternatively, for  $\varphi_A = \varphi_B$  it vanishes for arbitrary  $\tau$ . However,  $G_{\parallel}^{(12)}(t, t + \tau)$  does not vanish completely due to contributions from multiphoton signal excitations [second term in Eq. (6)]. To quantify the degree of the HOM effect, the following benchmark measurement is performed. We insert a half-wave plate into the path of the signal field from ensemble  $B$ , rotating its polarization from  $H$  to  $V$ , thus nullifying the HOM effect. Quantitatively, in this case the corresponding correlation function  $G_{\perp}^{(12)}(t, t + \tau)$  is given by Eq. (6), but now without the interference contributions (proportional to the product  $RT$ ) in the HOM term.

In our experiment two MOTs of  $^{85}\text{Rb}$  are used to provide optically thick atomic ensembles at sites  $A$  and  $B$  (Fig. 1). The ground levels  $\{|a\rangle; |b\rangle\}$  correspond to the  $5S_{1/2}$ ,  $F = \{3, 2\}$  levels of  $^{85}\text{Rb}$ , and the excited level  $|c\rangle$  represents the  $\{5P_{1/2}, F = 3\}$  level of the  $D_1$  line at 795 nm. For a linearly polarized write field we observe that the signal field is nearly orthogonally polarized, consistent with the theoretical value of  $\cos^2 \eta = 91/122$ , Eq. (2).

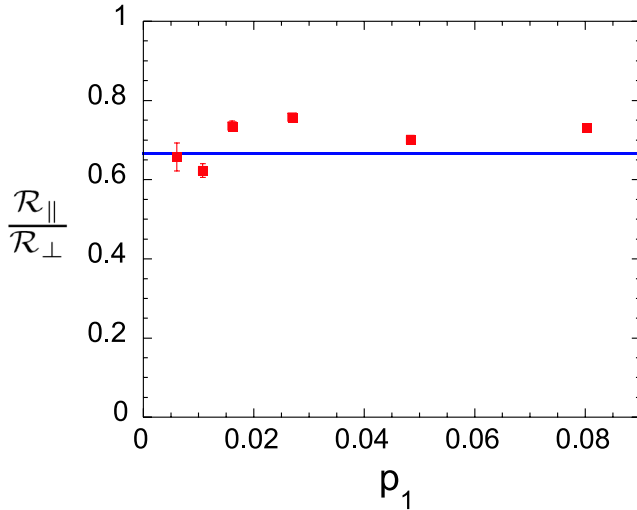


FIG. 2 (color online). Ratio of measured twofold coincidence rates for the  $\perp$  and  $\parallel$  configurations). The parameter  $p_1 \equiv (N_1 + N_2)/N_T$  (averaged over the  $\perp$  and  $\parallel$  cases). Here  $N_1(N_2)$  is the number of photoelectric detections in detector  $D1(D2)$ ,  $N_T$  is the number of experimental trials. Theoretically it can be expressed as  $p_1 = \epsilon_A s_A^2 + \epsilon_B s_B^2$ , where  $\epsilon_A(\epsilon_B) \approx 0.05\text{--}0.07$  is the overall probability to detect a signal photon from site  $A$  (site  $B$ ) by either  $D1$  or  $D2$ . The data acquisition time  $5 \text{ min} \leq T_D \leq 2 \text{ h}$  over the range of  $p_1$  values shown and  $N_T \equiv fT_D$ . Scatter beyond the estimated Poissonian level of uncertainty is consistent with systematic drifts in experimental conditions, in particular, the single count rates from each ensemble. The solid line is our theoretical prediction based on Eq. (6), for  $R = T = 1/2$  and  $\epsilon_A s_A^2 = \epsilon_B s_B^2$ .

To generate indistinguishable signal wave packets from the two atomic memories, we produce their respective write fields by splitting a single pulse and directing the outputs into identical 100 m long optical fibers. The two Raman-scattered signal fields produced at  $A$  and  $B$  are passed through polarizing cubes to select the  $H$  components and coupled into the ends of a fiber-based beam splitter. The outputs of the latter are connected to single-photon counting modules  $D1$  and  $D2$ . A half-wave plate is inserted into the path of signal field  $B$  (Fig. 1) which enables us to vary the relative (linear) polarization of the detected fields. This allows detection of the parallel polarizations ( $\parallel$ ), which exhibit the HOM effect, and orthogonal polarizations ( $\perp$ ), which do not.

Particular care is taken to eliminate possible sources of spectral broadening. Magnetic trapping fields are switched off after atomic collection and cooling, and the residual ambient field is compensated by sets of Helmholtz coils. All trapping and cooling light fields are switched off during data acquisition. The trapping light is shut off about  $10 \mu\text{s}$  before the repumping light, preparing unpolarized atoms in level  $|a\rangle$ . The repetition rate of the experiment  $f = 2 \times 10^5 \text{ s}^{-1}$ .

In Fig. 2 we show the measured ratio of the photoelectric coincidence rates  $\mathcal{R}_{\parallel}/\mathcal{R}_{\perp}$ , which are integrated over the duration of the write pulses. Our measurements exclude Rayleigh scattering on the write transition by means of frequency filtering. The experimental ratio  $\mathcal{R}_{\parallel}/\mathcal{R}_{\perp}$  is compared to the ratio of integrated correlation functions  $\iint dt d\tau G_{\parallel}^{(12)}(t, t + \tau)$  and  $\iint dt d\tau G_{\perp}^{(12)}(t, t + \tau)$ , assuming identical wave packets  $\varphi_A = \varphi_B$ . We observe scatter in the data beyond the level of the error bars. Since the latter are computed from the total numbers of counts in the  $\parallel$  and  $\perp$  configurations, assuming a Poissonian distribution, the scatter indicates the level of systematic drifts encountered over several hours of data acquisition.

The photoelectric coincidences arise from the signal field excitation pairs produced (i) one excitation from each ensemble; (ii) both excitations from ensemble  $A$ ; (iii) both excitations from ensemble  $B$ . The HOM visibility of  $V \equiv 1 - \mathcal{R}_{\parallel}/\mathcal{R}_{\perp} = \frac{1}{3}$  reflects the deleterious effects of contributions (ii) and (iii). These are relatively large because in the limit of weak excitation the spin wave-signal state is dominated by the vacuum contribution. By detecting the presence of a spin wave atomic excitation in each ensemble, these contributions could be substantially suppressed, and the HOM visibility  $V \rightarrow 1$  in the limit that the excitation probability  $p_1 \rightarrow 0$ .

We obtain high-visibility HOM fringes by means of a four-photon delayed coincidence detection procedure. This involves conversion of the spin wave excitation to an idler field by means of an incident read laser pulse which follows the write pulse by a programmable time delay  $\delta t$  in the off-axis geometry [19];  $\delta t$  is limited by the quantum memory coherence time  $\tau_c$  [20]. By careful minimization of ambient magnetic fields,  $\tau_c > 30 \mu\text{s}$  have been reported

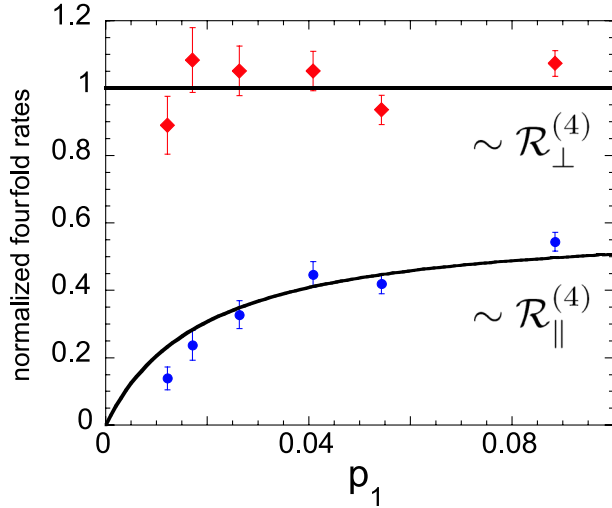


FIG. 3 (color online). Integrated fourfold coincidence rates  $\mathcal{R}_{\parallel}^{(4)}/\mathcal{W}_{\parallel}^{(4)}$  and  $\mathcal{R}_{\perp}^{(4)}/\mathcal{W}_{\perp}^{(4)}$  as a function of  $p_1$ . Experiment, dots, theory, solid line, assuming identical signal mode wave packets from each ensemble. Uncertainties are based on the statistics of the photon counting events.

[21]. In this work we choose  $\delta t = 100$  ns in order to maximize the repetition rate of the protocol. The fourfold detection of the two idler and two signal fields involves HOM of the two signal fields and delayed coincidence detection of the idler fields at detectors D3 and D4, as shown in Fig. 1.

The fourfold coincidence rate is thus given by

$$\mathcal{R}_{\parallel}^{(4)} \sim s_A^2 s_B^2 \{ (R - T)^2 (1 + 2s_A^2)(1 + 2s_B^2) + 2RT(3s_A^4 + 3s_B^4 + 2s_A^2 + 2s_B^2) \}. \quad (7)$$

We have again assumed identical wave-packet modes for both ensembles.

By inserting a half-wave plate into the path of the signal field from ensemble  $B$  as before (rotating polarization from  $H$  to  $V$ ), we suppress the HOM interference contributions, such that the fourfold coincidence rate becomes

$$\mathcal{R}_{\perp}^{(4)} \sim s_A^2 s_B^2 \{ (R^2 + T^2)(1 + 2s_A^2)(1 + 2s_B^2) + 2RT(3s_A^4 + 3s_B^4 + 2s_A^2 + 2s_B^2) \}. \quad (8)$$

In separate sets of measurements we recorded photoelectric events with one, or other, of the two MOTs blocked, which allow us to determine the expected level of fourfold coincidences for orthogonal polarizations of the two signal fields  $\mathcal{W}_{\perp}^{(4)}$  (i.e., in the absence of HOM). In Fig. 3 we plot  $\mathcal{R}_{\parallel}^{(4)}/\mathcal{W}_{\parallel}^{(4)}$  and  $\mathcal{R}_{\perp}^{(4)}/\mathcal{W}_{\perp}^{(4)}$  along with the corresponding theoretical predictions. HOM interference is manifested in that  $\mathcal{R}_{\parallel}^{(4)}/\mathcal{W}_{\parallel}^{(4)} \rightarrow 0$  as  $p_1 \rightarrow 0$ . The highest observed visibility  $V \equiv 1 - \mathcal{R}_{\parallel}^{(4)}/\mathcal{W}_{\parallel}^{(4)} \approx 0.86 \pm 0.03$ . As the theory and the experimental data agree within the statistical uncertainties, this indicates very good wave-

packet overlap of the signals produced by the remote ensembles.

In conclusion, we have demonstrated quantum interference of electromagnetic fields emitted by remote quantum memory elements separated by 5.5 m. Such high-visibility interference is an important element for entanglement distribution in proposed quantum network and distributed quantum computing systems [1,22–27].

We gratefully acknowledge illuminating discussions with M. S. Chapman. This work was supported by NSF, ONR, NASA, Alfred P. Sloan, and Cullen-Peck Foundations.

- 
- [1] E. Knill, R. Laflamme, and G.J. Milburn, *Nature* (London) **409**, 46 (2001).
  - [2] L.-M. Duan *et al.*, *Nature* (London) **414**, 413 (2001).
  - [3] T. Chanelière *et al.*, *Phys. Rev. Lett.* **96**, 093604 (2006).
  - [4] D.N. Matsukevich and A. Kuzmich, *Science* **306**, 663 (2004); similar results were reported in C. W. Chou *et al.*, *Nature* (London) **438**, 828 (2005).
  - [5] D.N. Matsukevich *et al.*, *Phys. Rev. Lett.* **95**, 040405 (2005); similar results were reported in H. de Riedmatten *et al.*, *Phys. Rev. Lett.* **97**, 113603 (2006).
  - [6] D.N. Matsukevich *et al.*, *Phys. Rev. Lett.* **96**, 030405 (2006).
  - [7] C.K. Hong, Z. Y. Ou, and L. Mandel, *Phys. Rev. Lett.* **59**, 2044 (1987).
  - [8] L. Mandel and E. Wolf, *Optical Coherence and Quantum Optics* (Cambridge University Press, Cambridge, U.K., 1995).
  - [9] C. Simon and W. T. M. Irvine, *Phys. Rev. Lett.* **91**, 110405 (2003).
  - [10] L. Mandel, *Rev. Mod. Phys.* **71**, S274 (1999).
  - [11] A. Zeilinger, *Rev. Mod. Phys.* **71**, S288 (1999).
  - [12] C. Santori *et al.*, *Nature* (London) **419**, 594 (2002).
  - [13] T. Legero, T. Wilk, M. Hennrich, G. Rempe, and A. Kuhn, *Phys. Rev. Lett.* **93**, 070503 (2004).
  - [14] J. Thompson *et al.*, *Science* **313**, 74 (2006).
  - [15] J. Beugnon *et al.*, *Nature* (London) **440**, 779 (2006).
  - [16] P. Maunz *et al.*, quant-ph/0608047.
  - [17] S.D. Jenkins, Ph.D. dissertation, Georgia Institute of Technology, 2006.
  - [18] A. Kuzmich and T.A.B. Kennedy, *Phys. Rev. Lett.* **92**, 030407 (2004).
  - [19] V. Balic *et al.*, *Phys. Rev. Lett.* **94**, 183601 (2005).
  - [20] T. Chanelière *et al.*, *Nature* (London) **438**, 833 (2005).
  - [21] D.N. Matsukevich *et al.*, *Phys. Rev. Lett.* **97**, 013601 (2006).
  - [22] H.J. Briegel, W. Dür, J.I. Cirac, and P. Zoller, *Phys. Rev. Lett.* **81**, 5932 (1998).
  - [23] H.J. Briegel and R. Raussendorf, *Phys. Rev. Lett.* **86**, 910 (2001).
  - [24] Y.L. Lim, A. Beige, and L.C. Kwek, *Phys. Rev. Lett.* **95**, 030505 (2005).
  - [25] S.D. Barrett and P. Kok, *Phys. Rev. A* **71**, 060310(R) (2005).
  - [26] Y.L. Lim *et al.*, *Phys. Rev. A* **73**, 012304 (2006).
  - [27] D.E. Browne and T. Rudolph, *Phys. Rev. Lett.* **95**, 010501 (2005).